Available online at www.sciencedirect.com
ScienceDirect
International Journal of Heat and Mass Transfer 51 (2008) 4168–4183
International Journal of HEAT and MASS TRANSFER
www.elsevier.com/locate/ijhmt

Intelligent fuzzy weighted input estimation method applied to inverse heat conduction problems

Tsung-Chien Chen [a,*], Ming-Hui Lee [b]

[a] Department of Power Vehicle and Systems Engineering, Chung Cheng Institute of Technology, National Defense University, Ta-shi, 190, Sanyuan 1st Street, Tao-Yuan 335, Taiwan, ROC
[b] School of Defense Science, Chung Cheng Institute of Technology, National Defense University, Ta-shi, 190, Sanyuan 1st Street, Tao-Yuan 335, Taiwan, ROC

Received 12 September 2007; received in revised form 21 February 2008
Available online 16 April 2008

Abstract

The innovative intelligent fuzzy weighted input estimation method which efficiently and robustly estimates the unknown time-varying heat flux in real-time is presented in this paper. The algorithm includes the Kalman Filter (KF) and the recursive least square estimator (RLSE), which is weighted by the fuzzy weighting factor proposed based on the fuzzy logic inference system. To directly synthesize the Kalman filter with the estimator, this work presents an efficient robust forgetting zone, which is capable of providing a reasonable compromise between the tracking capability and the flexibility against noises. The capability of this inverse method are demonstrated in one- and two-dimensional time-varying estimation cases and the proposed algorithm is compared by alternating between the constant and adaptive weighting factors. The results show that this method has the properties of faster convergence in the initial response, better target tracking capability and more effective noise reduction.

Keywords: Input estimation method; Kalman filter; Fuzzy weighting factor

1. Introduction

Utilizing the inverse techniques to estimate the thermal unknowns, such as boundary conditions, heat flux and thermal properties, has become a conventional means of resolving heat transfer problems in recent decades. When solving the inverse heat conduction problem, the inappropriate choice of the tuning parameter will cause an issue. The system is unstable, and extraordinarily sensitive to the measurement error. Besides, the thermal diffusion phenomenon contains the damping and lag effects. Various techniques have been developed to handle the inverse problems of heat conduction. Stolz [1], in 1957, provided one of the earliest numerical inverse solution algorithms for a quenching test. The inverse method is unstable and sensitive to the measurement errors due to the small time interval. Therefore, the solutions for IHCP should be able to reduce instability and sensitivity and provide the desired accuracy. Another solution for IHCP is the regularization method [2]. The regularization method was divided into the whole domain regularization algorithm and the conjugate gradient iterative algorithm. The whole domain regularization algorithm has been used by Miller in 1970 [3], Alifanov in 1974 [4], and Scott and Beck in 1989 [2]. The advantage of the algorithm is its simplicity in formulation. However, when the inverse algorithm is carried out over a long period of time, the number of dimensions of matrices and the computation load will increase gradually. The conjugate gradient iterative algorithm has been used by Alifanov and Millhailov in 1978 [5], Alifanov and Artyukhin in 1975 [6], and Mikhailov in 1983 [7]. The gradient iterative algorithm method has been proposed since the calculation procedure to solve the IHCP specified by the differential

* Corresponding author.
E-mail address: C2271003@ms61.hinet.net (T.-C. Chen).

0017-9310/$ - see front matter © 2008 Elsevier Ltd. All rights reserved.
doi:10.1016/j.ijheatmasstransfer.2008.02.026

Nomenclature

B	sensitivity matrix	$q(t)$	heat flux
$[B]$	gradient matrix	R	measurement noise covariance
$[C]$	capacitance matrix	R_o	radius of outer wall
C_p	specific heat	R_i	radius of inner wall
C_c	chrome specific heat	s	innovation covariance
C_s	steel specific heat	t	time
$[D]$	matrix of conductivity values	T	temperature
$\{F\}$	thermal load vector	T_0	initial temperature
$\{ff\}$	coefficient vector	v	measurement noise vector
H	measurement matrix	r	radial coordinate
I	identity matrix	$Z(k)$	observation vector
J	functional	γ	forgetting factor
J^e	element functional	α	thermal diffusivity
k	time (discretized)	α_c	thermal diffusivity of the chrome
k_c	chrome thermal conductivity	α_s	thermal diffusivity of the steel
k_s	steel thermal conductivity	Γ	input matrix
K	Kalman gain	σ	standard deviation
K_b	steady-state correction gain	δ	Dirac delta function
l	element length	ρ	density
M	sensitivity matrix	ρ_c	density of the chrome
$[M]$	global conductance matrix	ρ_s	density of the steel
N	total number of nodes	Φ	state transition matrix
$[N]$	shape function matrix	Ψ	coefficient matrix
P	filter's error covariance matrix	Ω	coefficient matrix
P_b	error covariance matrix	Δt	sampling time interval
Q	process noise covariance	ω	process noise vector

equations is interpreted as an optimal control theory. It has been utilized and investigated extensively by Huang and Ozisik [8–11], and Li and Yan [12,13]. The above-mentioned algorithms are based on either the batch or off-line form, which results in computational inefficiency.

In the industrial applications, some parameters of this problem must be determined on-line rather than in batch form. Therefore, Tuan et al. [14] successfully presented an input estimation approach which is recursive and on-line to solve the IHCPs. This method includes the Kalman filter and the recursive least square estimator. The heat conduction equation is transformed into the system state equation. The Kalman filter is used to generate the residual innovation sequence, and the real-time recursive least square algorithm is using this residual sequence to estimate the unknown time-varying inputs. In order to reduce the recollection capacity, the estimation data at the former time step and the measurement data in the current time step are applied to the estimation. In this work, the "on-line" form inverse methodology based on the concept of Kalman filtering is developed. The proposed method is a real-time recursive input estimation algorithm to estimate the unknown input. Therefore, the "off-line" technique of the batch form method to estimate the unknown time-varying input has been replaced by the proposed method. This technique is fairly adaptable in solving the IHCPs in real-time [15–17].

The weighting function is applied into the time-varying input estimation of the RLSE. The value of $\gamma(k)$ is a constant and heuristically chosen between 0 and 1. It performs as a tunable parameter which not only controls the bandwidth and magnitude of the RLSE gain, but also influences the lag in the time domain. A small value of $\gamma(k)$, although provides a good tracking ability, is influenced by the fluctuations due to uncertain system noise. On the contrary, a large value of $\gamma(k)$ is less sensitive to disturbances, but provides the relatively lower tracking ability to estimate the time-varying inputs. Therefore, the optimal selection of $\gamma(k)$ must be a trade-off between the required tracking capability and the acceptable noise sensitivity [18].

In the conventional estimation method, the optimal weighting factor is obtained only through complicated estimation process analysis [18]. The innovation sequences imply the effect of the unknown input. For instance, when there is no input yet, the bias-free innovation sequence demonstrates this situation. On the other hand, when an unknown input acts on the boundary, the bias innovation sequence from the Kalman filter will show the existence and quantity of this unknown input [19]. The bias innovation sequence is observable and analogous to the unknown

input when the error covariance of estimation is sufficiently small. In the meantime, by assuming the weighting function to be a function of innovation, an adaptive estimation process can be obtained. Although the input estimates converge slowly in the initial time when the adaptive weighting function is used in the RLSE, the estimator has good overall tracking performance when the unknown input is time-varying regardless of the influence of the measurement noise interference [20].

In this paper, an intelligent fuzzy weighting function is used to replace the weighting factor, $\gamma(k)$, of the RLSE. Improving the weighting efficiency of the RLSE is essential, because the unknown input is time-varying and changes continuously. The adaptive weighting function takes any input variation into account. Therefore, the inverse method with quick target tracking and effective noise reduction is developed. The heat conduction equation is transferred to the state equation. The unknown input heat flux is assumed as the unknown parameter. The operation of input estimation method is first to measure the outer wall temperature state. In the meantime, the Kalman Filter is used to generate the residual innovation sequence. The residual innovation sequence connotes the biased or systematic error due to the unknown time-varying input items, variance or random error form the measurement. The estimator then estimates the histories of unknown heat flux by applying the residual innovation sequence to the intelligent fuzzy weighted recursive least square algorithm. In other word, the unknown input parameter in any form of the unknown input item can be estimated.This inverse method presents an efficient and robust estimation procedure to any unknown input situation. The presented work addresses an intelligent fuzzy weighted estimator based on the fuzzy logic system. The robustness and efficiency of this method will be demonstrated through three simulation case studies. The results are also compared with the ones using other algorithms. The reliability, adaptivity, and robustness of this method can therefore be verified.

2. Problem formulation

Assuming that there is a hollow composite pipe, the radius of the inner and outer walls are R_i and R_o, respectively. The radius of the interface between the two metal layers is R_L. $d_c(\equiv R_L - R_i)$ is the thickness of the chrome layer. The temperature measurement, $z(t)$, is measured by the thermocouple at $x = R_o$. Fig. 1 shows the geometry of the system structure.

The restrictions are as follows [21]:

(1) The temperature distribution in the axial direction is neglected because it is relatively small in comparison to that in the radial direction.
(2) The temperature distribution is axis-symmetrical in the plane normal to the pipe axis. It means that the heat input is also axis-symmetrical, and the gravity in the barrel wall and chrome thickness variation along with other effects that would cause dissymmetry are neglecting.
(3) The thermal expansion of the pipe is not considered in the heat transfer process.
(4) The densities, specific heats, and thermal conductivities of steel and chrome layers are assumed as constants.
(5) Thermally perfect conjunction is assumed at the chrome–steel interface (i.e., the temperature distribution and radial conductive heat flux are both continuous).
(6) The latent heat effects due to the phase change of steel from martensite to austenite are neglected.
(7) The mathematical formulation of the one-dimensional transient heat conduction problem can be generalized as follows [17]:

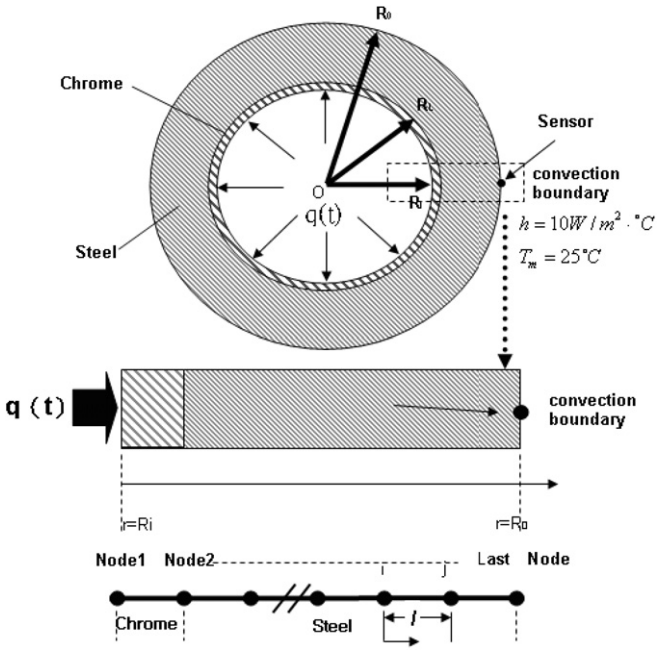

Fig. 1. System geometry [17].

$$\frac{\partial^2 T(r,t)}{\partial r^2} + \frac{1}{r}\frac{\partial T(r,t)}{\partial r} = \left(\frac{1}{\alpha_c}\right)\frac{\partial T(r,t)}{\partial t} \quad \text{in } R_i \leqslant r \leqslant R_L, \tag{1}$$

$$\frac{\partial^2 T(r,t)}{\partial r^2} + \frac{1}{r}\frac{\partial T(r,t)}{\partial r} = \left(\frac{1}{\alpha_s}\right)\frac{\partial T(r,t)}{\partial t} \quad \text{in } R_L \leqslant r \leqslant R_o, \tag{2}$$

$$T(r,0) = T_0 \quad \text{for } t = 0 \text{ in } R_i \leqslant r \leqslant R_o, \tag{3}$$

$$-k_c\frac{\partial T}{\partial r} = q(t) \quad \text{in } r = R_i, \tag{4}$$

$$-k_s\frac{\partial T}{\partial r} = h(T - T_\infty) \quad \text{in } r = R_o, \tag{5}$$

$$k_c\left(\frac{\partial T}{\partial r}\right)_c = k_s\left(\frac{\partial T}{\partial r}\right)_s \quad \text{in } r = R_L, \tag{6}$$

$$Z(r,t) = T(r,t) + v(t) \quad \text{measured temperature}, \tag{7}$$

T is the temperature distribution as a function of r and t. t is the elapsing time from the initiation. The constants $\alpha_c \equiv k_c/(\rho_c \cdot c_{p_c})$ and $\alpha_s \equiv k_s/(\rho_s \cdot c_{p_s})$ are the thermal diffusivities of the chrome and steel, respectively. k_c, ρ_c, and c_{p_c} are the thermal conductivity, density, and specific heat of chrome, respectively; k_s, ρ_s, and c_{p_s} are the corresponding properties of steel.

T_0 is the uniform initial temperature. $q(t)$ is the unknown heat flux input to be estimated. $Z(t)$ is the noise-corrupted measurement. $v(t)$ is the measurement noise assumed as Gaussian white noise with zero mean. h is the convection coefficient when the heat transfers between the barrel wall and the surrounding atmosphere. T_∞ is the temperature on the outer wall.

In the chrome layer where $R_i \leqslant r \leqslant R_L$, the calculus of variations provides an alternative method for formulating the governing equation (1) and boundary conditions (3, 4, and 6). Variation calculus illustrates the minimization of the functional J_c [22]:

$$J_c = \frac{1}{2}\int_V\int\int\left[rk_c\cdot\left(\frac{\partial T}{\partial r}\right)^2 + 2r\rho_c C_c\cdot\left(\frac{\partial T}{\partial t}\right)\cdot T\right]dV + \int_S qT\,dS. \tag{8}$$

The element equation for the temperature is

$$T^e = N_i^e T_i + N_j^e T_j = [N^e]\{T\},$$

where T_i and T_j are the node temperatures to be determined:

$$[N^e] = \begin{bmatrix} N_i^e & N_j^e \end{bmatrix} = \begin{bmatrix} \frac{R_j - r}{R_j - R_i} & \frac{r - R_i}{R_j - R_i} \end{bmatrix}.$$

The temperature gradient matrix, $\{g^e\}$, is given by

$$\begin{aligned}\{g^e\} &= \frac{\partial T^e}{\partial r} = \begin{bmatrix} \frac{\partial N_i^e}{\partial r} & \frac{\partial N_j^e}{\partial r} \end{bmatrix}\{T\} \\ &= -\frac{1}{R_j - R_i}T_i + \frac{1}{R_j - R_i}T_j \\ &= \begin{bmatrix} -\frac{1}{R_j - R_i} & \frac{1}{R_j - R_i} \end{bmatrix}\begin{Bmatrix} T_i \\ T_j \end{Bmatrix} \\ &= [B^e]\{T\},\end{aligned}$$

where $[N]$ is the shape function matrix, and $[B]$ is obtained by differentiating $[N]$ with respect to r.

Eq. (8) must be minimized with respect to the set of nodal value $\{T\}$

$$\frac{\partial J_c}{\partial\{T\}} = \frac{\partial}{\partial\{T\}}\sum_{e=1}^{E} J_c^e = \sum_{e=1}^{E}\frac{\partial J_c^e}{\partial\{T\}} = 0.$$

The minimization process produces the following equation:

$$[C]_c\frac{\partial\{T\}}{\partial t} + [M]_c\{T\} + \{F\}_c = 0.$$

The $[C]_c$ matrix is the global capacitance matrix. $[M]_c$ is the global conductance matrix. $\{F\}_c$ is the thermal load vector. The element of $[C]_c$, $[M]_c$, and $\{F\}_c$ are summarized as follows:

$$[D^e]_c = [rk_c^e], \tag{9}$$

$$\begin{aligned}[C^e]_c &= \int_V r\rho_c C_c[N^e]\{T\}[N^e]\frac{\partial\{T\}}{\partial t}dV \\ &= \frac{2\pi\rho_c C_c}{60l^2}\begin{bmatrix} (2R_j^5 - 20R_j^2R_i^3 + 30R_jR_i^4 - 12R_i^5) & & \\ (3R_j^5 - 5R_j^4R_i + 5R_jR_i^4 - 3R_i^5) & (3R_j^5 - 5R_j^4R_i + 5R_jR_i^4 - 3R_i^5) & \\ (12R_j^5 - 30R_j^4R_i + 20R_j^3R_i^2 - 2R_i^5) & & \end{bmatrix},\end{aligned} \tag{10}$$

$$\begin{aligned}[M^e]_c &= \int_V [B^e]^T[D^e]_c[B^e]dV \\ &= \frac{2\pi k_c}{l^2}\int_{R_i}^{R_j}\begin{bmatrix} -1 \\ 1 \end{bmatrix}[-1 \quad 1]r^2\,dr \\ &= \frac{2\pi k_c(R_j^3 - R_i^3)}{3(R_j - R_i)^2}\begin{bmatrix} 1 & -1 \\ -1 & 1 \end{bmatrix},\end{aligned} \tag{11}$$

$$\{f^e\}_c = \int_{S_1} q[N^e]^T\,dS = \{ff\}q = 2\pi R_i q\begin{bmatrix} 1 \\ 0 \end{bmatrix}, \tag{12}$$

R_i and R_j are the single elements of the left node and right node. The length between the single elements, $l = R_j - R_i$. $[D]$ is the matrix composed of the conductivity values. $[ff]$ is the coefficient matrix.

In the steel layer, The functional formula that is equivalent to Eq. (2) and its boundary conditions, Eqs. (3), (5) and (6) is J_s:

$$J_s = \frac{1}{2}\int_V\int\int\left[rk_s\cdot\left(\frac{\partial T}{\partial r}\right)^2 + 2r\rho_s C_s\cdot\left(\frac{\partial T}{\partial t}\right)\cdot T\right]dV + \int_{S_1}\frac{1}{2}h(T - T_\infty)^2\,dS, \tag{13}$$

$$J = \sum_{e=1}^{E}\int_{V^e}\frac{1}{2}\{g^e\}^T[D^e]\{g^e\}dV + \int_V r(\rho_s C_s)^e\left(\frac{\partial T^e}{\partial t}\right)T^e\,dV + \int_{S_1^e}\frac{1}{2}h(T^e - T_\infty^e)^2\,dS, \tag{14}$$

where E is the number of elements, e is the single element. Therefore

$$J_s = J_s^1 + J_s^2 + \cdots + J_s^E = \sum_{e=1}^{E} J_s^e.$$

A single element can be extracted as the following:

$$\begin{aligned}J_s^e &= \int_{V^e}\frac{1}{2}\{T\}^T\{B^e\}^T[D^e]\{B^e\}\{T\}dV \\ &+ \int_{V^e} r\rho_s C_s[N^e]\{T\}[N^e]\frac{\partial\{T\}}{\partial t}\,dV \\ &+ \int_{S_1^e}\frac{h}{2}\{T\}^T\{N^e\}^T\{N^e\}\{T\}\,dS - \int_{S_1^e} hT_\infty\{N^e\}\{T\}\,dS \\ &+ \int_{S_1^e}\frac{h}{2}hT_\infty^2\,dS\end{aligned} \tag{15}$$

In the steel layer, Eq. (15) needs to be minimized with respect to the set of nodal values $\{T\}$:

$$\frac{\partial J_s}{\partial\{T\}} = \frac{\partial}{\partial\{T\}}\sum_{e=1}^{E} J_s^e = \sum_{e=1}^{E}\frac{\partial J_s^e}{\partial\{T\}} = 0.$$

We can determine the steel layer single element matrix $[C^e]_s$, $[M^e]_s$, and $\{f^e\}_s$ as follows:

$$[D^e]_s = [rk_s^e], \tag{16}$$

$$\begin{aligned}[C^e]_s &= \int_V r\rho_s C_s [N^e]\{T\}[N^e]\frac{\partial\{T\}}{\partial t}\,dV \\ &= \frac{2\pi\rho_s C_s}{60l^2}\begin{bmatrix} (2R_j^5 - 20R_j^2R_i^3 + 30R_jR_i^4 - 12R_i^5) & & \\ (3R_j^5 - 5R_j^4R_i + 5R_jR_i^4 - 3R_i^5) & & \\ (3R_j^5 - 5R_j^4R_i + 5R_jR_i^4 - 3R_i^5) & & \\ (12R_j^5 - 30R_j^4R_i + 20R_j^3R_i^2 - 2R_i^5) & & \end{bmatrix},\end{aligned} \tag{17}$$

$$\begin{aligned}[M^e]_s^1 &= \int_V [B^e]^T[D^e]_s[B^e]\,dV \\ &= \frac{2\pi k_s}{l^2}\int_{R_i}^{R_j}\begin{bmatrix}-1\\1\end{bmatrix}[-1 \quad 1]r^2\,dr \\ &= \frac{2\pi k_s(R_j^3 - R_i^3)}{3(R_j - R_i)^2}\begin{bmatrix}1 & -1\\ -1 & 1\end{bmatrix}.\end{aligned} \tag{18}$$

At the right node ($N_i = 0$, $N_j = 1$, $r = R_j$)

$$\begin{aligned}[M^e]_s^2 &= \int_{S_2^e} h\{N^e\}^T\{N^e\}\,dS \\ &= \int_{S_2^e} h\begin{bmatrix}N_iN_i & N_jN_i\\ N_iN_j & N_jN_j\end{bmatrix}dSS \\ &= 2\pi R_o h\begin{bmatrix}0 & 0\\ 0 & 1\end{bmatrix}.\end{aligned}$$

Merging the ms in $[M^e]_s^1$ for element $1,2,\ldots,n.$ and $[M^e]_s^2$ into the global conductance matrix, $[M]_s$:

$$[M]_s = \begin{bmatrix} m_1 & -m_1 & 0 & 0 & 0 & 0\\ -m_1 & m_1+m_2 & -m_2 & 0 & 0 & 0\\ 0 & -m_2 & m_2+m_3 & -m_3 & 0 & 0\\ 0 & 0 & -m_3 & m_3+m_4 & \cdots & \cdots\\ \cdots & \cdots & \cdots & \cdots & \ddots & -m_n\\ 0 & 0 & 0 & 0 & -m_n & m_n + 2\pi R_o h\end{bmatrix}, \tag{19}$$

$$\begin{aligned}\{f^e\}_c &= \int_{S_1^e} hT_\infty\{N^e\}^T\,dS = \int_{S_1^e} hT_\infty\begin{bmatrix}0\\1\end{bmatrix}dS \\ &= 2\pi R_o\cdot hT_\infty\begin{bmatrix}0\\1\end{bmatrix}.\end{aligned} \tag{20}$$

Assembling the chrome layer and the steel layer, and minimizing it with respect to the set of nodal values, $\{T\}$:

$$\frac{\partial J}{\partial\{T\}} = \frac{\partial}{\partial\{T\}}\sum_{e=1}^{E} J^e = \sum_{e=1}^{E}\frac{\partial J^e}{\partial\{T\}} = 0. \tag{21}$$

Eq. (21) is the first-order linear differential equation of the system:

$$[C]\frac{\partial\{T\}}{\partial t} + [M]\{T\} + \{F\} = 0, \tag{22}$$

$[C]$ matrix is the capacitance matrix. $[M]$ is the conductance matrix. $\{F\}$ is the thermal load vector. According to Eq. (22), by taking the process noise inputs [23] into account, the continuous-time state equation can be obtained as follows:

$$\begin{aligned}&\dot{\mathrm{T}}(t) = \Psi\mathrm{T}(t) + \Omega[q(t) + w(t)], \\ &\Psi = (-1)[C]^{-1}[M], \\ &\Omega = (-1)[C]^{-1}\{ff\}.\end{aligned} \tag{23}$$

The state vector $T(t)$ is $N\times 1$. N is the total number of nodes. Ψ and Ω are the coefficient matrices. Ψ is $N\times N$. Ω is $N\times 1$. $q(t)$ is the unknown heat flux input on the boundary. $\omega(t)$ is the process noise. This noise term represents the modeling error. The state equation can be sampled with the time interval, Δt:

$$X(k) = \Phi X(k-1) + \Gamma[q(k-1) + \omega(k-1)], \tag{24}$$

where

$$\begin{aligned}&X(k-1) = [\,T_1 \quad T_2 \quad T_3 \quad \cdots \quad T_{N-1} \quad T_N\,]^T, \\ &\Phi = \mathrm{e}^{\Psi\Delta t}, \\ &\Gamma = \int_{k\Delta t}^{(k+1)\Delta t}\exp\{\Psi[(k+1)\Delta t - t]\}\Omega\,dt,\end{aligned}$$

X represents the state vector. Φ is the state transition matrix. Γ is the input matrix. q is the input sequence. ω is the process noise vector, which is assumed to be white noise with zero mean. The variance is as following:

$$E\{\omega(k)\omega^T(j)\} = Q\delta_{kj}, \tag{25}$$

where δ_{kj} is a Dirac delta function. In order to compare the results for situations involving measurement errors, Eq. (8) is adopted. The discrete-time measurement equation becomes

$$Z(k) = HX(k) + v(k), \tag{26}$$

Z is the observation vector at time $k\Delta\tau$. H is the measurement matrix. v is the measurement noise vector, which is assumed to be white. The variance of $v(k)$ is given by $E\{v(k)v^T(j)\} = R\delta_{kj}$.

The conventional input estimation approach has two parts: one is the Kalman filter without the input term, and the other is the weighted recursive least square estimator. The detailed formulation of this technique can also be found in Tuan et al. [14].

The equations of the Kalman filter are as follows:

$$\overline{X}(k/k-1) = \Phi\overline{X}(k-1/k-1), \tag{27}$$

$$P(k/k-1) = \Phi P(k-1/k-1)\Phi^{\mathrm{T}} + \Gamma Q\Gamma^{\mathrm{T}}, \tag{28}$$

$$s(k) = HP(k/k-1)H^{\mathrm{T}} + R, \tag{29}$$

$$K(k) = P(k/k-1)H^{\mathrm{T}}s^{-1}(k), \tag{30}$$

$$P(k/k) = [I - K(k)H]P(k/k-1), \tag{31}$$

$$\overline{Z}(k) = Z(k) - H\overline{X}(k/k-1), \tag{32}$$

$$\overline{X}(k/k) = \overline{X}(k/k-1) + K(k)\overline{Z}(k). \tag{33}$$

The equations of the recursive least squares estimator are as follows:

$$B(k) = H[\Phi M(k-1) + I]\Gamma, \tag{34}$$

$$M(k) = [I - K(k)H][\Phi M(k-1) + I], \tag{35}$$

$$K_b(k) = \gamma^{-1}P_b(k-1)B^{\mathrm{T}}(k) \times [B(k)\gamma^{-1}P_b(k-1)B^{\mathrm{T}}(k) + s(k)]^{-1}, \tag{36}$$

$$P_b(k) = [I - K_b(k)B(k)]\gamma^{-1}P_b(k-1), \tag{37}$$

$$\hat{q}(k) = \hat{q}(k-1) + K_b(k)[\overline{Z}(k) - B(k)\hat{q}(k-1)]. \tag{38}$$

$\hat{q}(k)$ is the estimated input vector. $P_b(k)$ is the error covariance of the estimated input vector. $B(k)$ and $M(k)$ are the sensitivity matrices. $K_b(k)$ is the correction gain. $\overline{Z}(k)$ is the bias innovation produced by the measurement noise and input disturbance. $s(k)$ is the covariance of the residual. γ is the weighting constant or weighting factor.

3. The intelligent fuzzy weighted RLSE input estimation approach

In this section, the intelligent fuzzy weighting factor is constructed. It can be operated at each step based on the innovation from the Kalman filter. The thermal unknown is assumed to be constant with the value of q_{k-1} over the time steps, $k = 0, 1, \ldots, n, n+1, \ldots, n+l, \ldots$ as follows:

$$q(k-1) = \begin{cases} 0, & k-1 < n, \\ q_{k-1}, & n < k-1 < n+l. \end{cases} \tag{39}$$

Although q_{k-1} is unknown, the important recursive relation has already been derived as follows [14]:

$$\overline{Z}(k) = \begin{cases} \widehat{Z}(k), & k-1 \leqslant n, \\ \widehat{Z}(k) + B(k)q_{k-1}, & n < k-1 \leqslant n+l, \end{cases} \tag{40}$$

where $\widehat{Z}(k) = Z(k) - H\widehat{X}(k/k-1)$ denotes the bias-free innovations caused by the measurement noise. The noises, $\widehat{Z}(1)$ to $\widehat{Z}(k)$, are assumed to be independent and to have the same distribution, that is to say, they are Gaussian white noises with zero means.

$\overline{Z}(k) = Z(k) - H\overline{X}(k/k-1)$ is the bias innovation caused by measurement noise and input bias. According to Eq. (40), $\overline{Z}(k)$ is white or normally distributed when there is no input. Note that the unknown input q_{k-1} can generally be arbitrary (deterministic or random). When q_{k-1} starts to act on the system, $\overline{Z}(k)$ can be assumed to be abnormally or long-tail distributed if the input is considered to have a large deviation.

In the equations of the recursive least square estimator, $\hat{q}(k)$ is the estimate of the unknown input. $P_b(k)$ is the error covariance of the input estimation process. $K_b(k)$ is the correction gain. $\gamma(k)$ is the weighting factor in the range between 0 and 1. The two functions of $\gamma(k)$ are smoothing and forgetting. The forgetting effectiveness depends on the value of $\gamma(k)$. $K_b(k)$ gets larger as $\gamma(k)$ gets smaller according to Eq. (36). The forgetting effect becomes more conspicuous according to Eq. (37). Note that the faster the forgetting effect is, the lower the smoothing effect will be, that is, it introduces oscillation. The weighting factor $\gamma(k)$ is employed to compromise between the upgrade of tracking capability and the loss of estimation precision. The relation has already been derived as follows [14]:

$$\gamma(k) = \begin{cases} 1, & |\overline{Z}(k)| \leqslant \sigma, \\ \frac{\sigma}{|\overline{Z}(k)|}, & |\overline{Z}(k)| > \sigma. \end{cases} \tag{41}$$

The weighting factor, $\gamma(k)$, as shown in Eq. (41) is adjusted according to the measurement noise and input bias. In the industrial applications, the standard deviation σ is set as a constant value. The magnitude of weighting factor is determined according to the modulus of bias innovation, $|\overline{Z}(k)|$. The unknown input prompt variation will cause the large modulus of bias innovation. In the meantime, the smaller weighting factor is obtained when the modulus of bias innovation is larger. Therefore, the estimator accelerates the tracking speed and produces larger vibration in the estimation process. On the contrary, the smaller variation of unknown input causes the smaller modulus of bias innovation. In the meantime, the larger weighting factor is obtained according to the small modulus of bias innovation. The estimator is unable to estimate the unknown input effectively. For this reason, the intelligent fuzzy weighting factor for the inverse estimation method which efficiently and robustly estimates the time-varying unknown input will be constructed in this research.

The basic configuration of the fuzzy logic system considered in this paper is illustrated here. The fuzzy logic system includes four basic components: the fuzzy rule base, fuzzy inference engine, fuzzier, and defuzzier. The range of fuzzy logic system input, $\theta(k)$, may be chosen in the interval, $[0, 1]$:

$$\theta(k) = \frac{|\Delta\overline{Z}(k)|}{\sqrt{\Delta\overline{Z}^2(k) + \Delta t^2}}, \tag{42}$$

where $\Delta\overline{Z}(k) = \overline{Z}(k) - \overline{Z}(k-1)$ denotes the variations of the bias innovation. Δt is the sampling interval. The proposed intelligent fuzzy weighting factor uses the input variable $\theta(k)$ to self-adjust the factor $\gamma(k)$ of the recursive least squares estimator. Therefore, the fuzzy logic system consists of one input and one output variables. The range of input, $\theta(k)$, may be chosen in the interval, $[0, 1]$, and the range of output, $\gamma(k)$, may also be in the interval, $[0, 1]$. The fuzzy sets for $\theta(k)$ and $\gamma(k)$ are labeled in the linguistic terms of EP (extremely large positive), VP (very large positive), LP (large positive), MP (medium positive), SP (small positive), VS (very small positive), and ZE (zero). The spe-

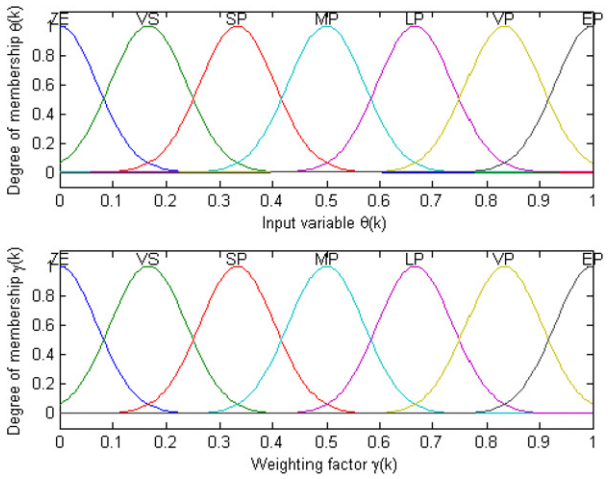

Fig. 2. Membership functions for the fuzzy sets for $\theta(k)$ and $\gamma(k)$ [27].

cific membership is defined by using Gaussian functions shown in Fig. 2.

A fuzzy rule base is a collection of fuzzy IF–THEN rules [27]:

IF $\theta(k)$ is zero (ZE) THEN $\gamma(k)$ is extremely large positive (EP),
IF $\theta(k)$ is very small positive (VS) THEN $\gamma(k)$ is very large positive (VP),
IF $\theta(k)$ is small positive (SP) THEN $\gamma(k)$ is large positive (LP),
IF $\theta(k)$ is medium positive (MP) THEN $\gamma(k)$ is medium positive (MP),
IF $\theta(k)$ is large positive (LP) THEN $\gamma(k)$ is small positive (SP),
IF $\theta(k)$ is very large positive (VP) THEN $\gamma(k)$ is very small positive (VS),
IF $\theta(k)$ is extremely large positive (EP) THEN $\gamma(k)$ is zero (ZE),

where $\theta(k) \in U$ and $\gamma(k) \in V \subset R$ are the input and output of the fuzzy logic system, respectively.

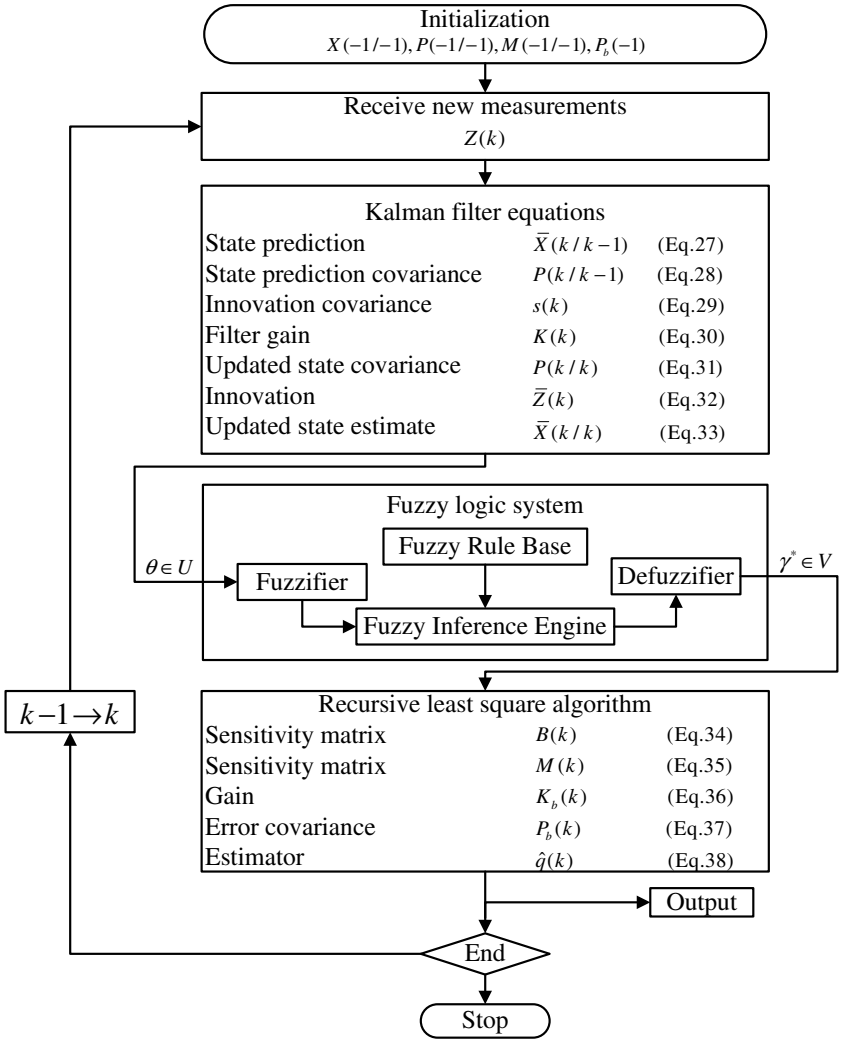

Fig. 3. Flow chart of the intelligent fuzzy weighted input estimation algorithm [27].

The fuzzier maps a crisp point $\theta(k) \in U$ into a fuzzy set A in U. Therefore, the nonsingleton fuzzier can be expressed in [24]:

$$\mu_A(\theta(k)) = \exp\left(-\frac{(\theta(k)-\bar{x}_i^l)^2}{2(\sigma_i^l)^2}\right), \tag{43}$$

$\mu_A(\theta(k))$ decreases from 1 as $\theta(k)$ moves away from $\bar{x}_i^l$. $(\sigma_i^l)^2$ is a parameter characterizing the shape of $\mu_A(\theta(k))$.

The fuzzy inference engine performs mapping from fuzzy sets in U to B in R based on the fuzzy IF–THEN rules and the compositional rule of inference. The Mamdani maximum–minimum inference engine was used in this paper. The max–min-operation rule of fuzzy implication is shown in [24]:

$$\mu_B(\gamma(k)) = \max_{j=1}^{c}\left\{\min_{i=1}^{d}[\mu_{A_i^j}(\theta(k)), \mu_{A_i^j \to B^j}(\theta(k),\gamma(k))]\right\}, \tag{44}$$

where c is the fuzzy rule, and d is the dimension of input variables.

The defuzzier maps a fuzzy set B in V to a crisp point $\gamma \in V$. The fuzzy logic system with the center of gravity is defined in [24]:

$$\gamma^*(k) = \frac{\sum_{l=1}^{n}\bar{\gamma}^l \mu_B(\gamma^l(k))}{\sum_{l=1}^{n}\mu_B(\gamma^l(k))}, \tag{45}$$

n is the number of outputs. $\bar{\gamma}^l$ is the value of the lth output. $\mu_B(\gamma^l(k))$ represents the membership of $\gamma^l(k)$ in the fuzzy set B. Using $\gamma^*(k)$ in Eq. (45) to replace in Eqs. (36) and (37) allows us to configure an adaptive fuzzy weighting function of the recursive least square estimator (RLSE). A flow chart of the computation for the application of the recursive input estimation algorithm is given in Fig. 3.

4. Results and discussion

To verify the performance of the proposed method, a thermal fluid flowing into the hollow cylinder pipe is modeled. The heat flux on the inner wall is estimated inversely by measuring the temperature on the outer wall. The thermal and mechanical properties of the hollow cylinder pipe steel (AISI 4340) and its associated chrome layer are shown as Table 1 [21]. The inner and outer diameters of the double-layer hollow cylinder pipe are $R_i = 0.020$ m, and $R_o = 0.025$ m. The thickness of chrome is 0.5 mm.

Two typical heat flux inputs are considered in the proposed approach. A thermocouple was placed at $x = R_o$ on the outer wall. The convection heat transfer coefficient is not a property of the fluid. It is an experimentally determined parameter whose value depends on all the variables influencing convection, such as the surface geometry, the nature of fluid motion, the properties of the fluid, and the bulk fluid velocity. Several typical values of are given in Tables 1–5 of [25]. Tables 1–5 show that the free convection heat transfer coefficient of air. Therefore, the free convection heat transfer coefficient of air, is set as the simulation condition. In general, the free convection heat transfer coefficient is assumed according to the real experiment situation. Different total time periods, $t_f = 8$ s and 12 s; the sampling interval, $\Delta t = 0.01$ s; the number of elements, $E = 10$; the process noise covariance matrix, $Q = 10^4$; the measurement noise covariance matrix, $R = \sigma^2 = 10^{-8}$, where σ is the standard deviation of the noise. The initial conditions for the input estimator are given as follows:

$$X(-1/-1) = [0 \quad 0 \quad \cdots \quad 0]^{\mathrm{T}} \text{ and } P(-1/-1) = \mathrm{diag}[10^8].$$

For the Kalman filter:

$q(-1) = 0$, and $P_b(-1) = 10^8$. $M(-1)$ is set as a zero matrix for the real-time least square estimator. Since $P(-1/-1)$ and $P_b(-1)$ are normally unknown, $P(-1/-1)$ and $P_b(-1)$ of the estimator can be initialized as large numbers. This has the effect of treating the initial errors as large numbers, so that the estimator usually ignores the first few estimates. The measurement of the unknown input heat flux, $q(t)$, on the inner wall surface is simulated by adding the measurement error to the actual temperature, which is solved directly from the heat conduction equation:

$$Z(t,r) = T(t,r) + \omega\sigma, \tag{46}$$

where ω is a random variable in the range that $-2.576 \leqslant \omega \leqslant 2.576$. Two test input heat fluxes are chosen as the transient and continuous square waveforms.

Example 1. Transient square waveform for $q(t)$ (W/m^2).

The input heat flux is modeled by a transient square waveform which flows into the hollow cylinder pipe. The transient square waveform denotes three rounds in one shot. $q(t)$ is shown as the following:

$$q(t) = \begin{cases} 7\times 10^5, & 3 \leqslant t \leqslant 3.25 \\ 0, & \text{otherwise.} \end{cases} \tag{47}$$

The thermocouple is located on the outer wall of the hollow cylinder pipe. The process noise covariance matrix, $Q = 10^4$, and the measurement noise covariance matrix, $R = \sigma^2 = 10^{-8}$. The estimates of $q(t)$ using the intelligent fuzzy weighting function, the adaptive weighting function, and the constant weighting factor, $\gamma = 0.95$, are plotted in Fig. 4. The estimation results show that the estimators with the intelligent fuzzy weighting function and the constant weighting factor have quicker convergence performance than that with the adaptive weighting function. A great quantity of unknown heat flux input is applied on the inner wall of the hollow cylinder pipe. The adaptive weighted

Table 1
Thermal and mechanical properties of materials

	Chrome	Steel (AISI 4340)
Specific heat	$C_c = 505.03$ J/(kg K)	$C_s = 469.05$ J/(kg K)
Density	$\rho_c = 7191$ kg/m^3	$\rho_s = 7827$ kg/m^3
Thermal conductivity	$k_c = 83.75$ J/(m s K)	$k_s = 38.07$ J/(m s K)
Thermal diffusivity	$\alpha_c = 2.305\times 10^{-5}$ m^2/s	$\alpha_s = 1.037\times 10^{-5}$ m^2/s
Melting temperature	$(T_m)_c = 2130$ K	$(T_m)_s = 1777$ K

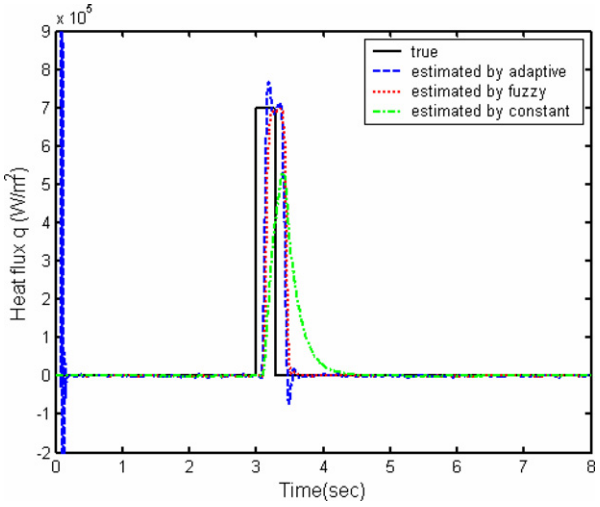

Fig. 4. Comparison of the inverse estimation using different weighting functions when the input is a single square heat flux wave ($Q = 10^4$, $R = 10^{-8}$).

estimator has great tracking performance, but it is not suitable in reducing the effect of the measurement noise. On the contrary, the constant weighted estimator has good performance in reducing the effect of the measurement noise, but it produces estimates with lower precision. The simulation results demonstrate that the proposed estimation method has great performance in convergence in the initial stage and in reducing the effect of measurement noise.

Fig. 5 shows that the estimator is influenced by the correction gain, K_b, in the estimation process. The largest correction gain is adopted by the adaptive weighting function of the estimator. The second is adopted by intelligent fuzzy weighting function and the smallest is adopted by the constant weighting factor. The adaptive weighted estimator uses the larger correction gain to maintain the tracking capability for a great quantity of unknown input. However, the capability in reducing the influence of measurement noise is not quite efficient. On the contrary, the constant weighted estimator has the opposite effect. The intelligent fuzzy weighted estimator is using a reasonable correction gain to obtain rapider convergence in the initial response stage and higher tracking performance, and to reduce the influence of measurement noise. This work presents a robust forgetting zone, capable of providing a reasonable trade-off between the tacking capability and the flexibility against noises to maintain the effectiveness of estimation process.

Fig. 6 shows that the estimator would be influenced by the error covariance, P_b in the estimation process. The largest error covariance is adopted by the adaptive weighting function of the estimator. The second is adopted by the intelligent fuzzy weighting function and the smallest is adopted by the constant weighting factor. The adaptive weighted estimator uses the larger error covariance to maintain the tracking capability for a great quantity of unknown input. However, the capability in reducing the influence of measurement noise is not quite efficient. On the contrary, the constant weighting estimator has the opposite effect. According to the effects mentioned above, the error covariance and the correction gain have the same effects to the estimator.

According to Fig. 7 and Eqs. (36)–(38), $\hat{q}(k)$ is the estimate of the unknown input. $P_b(k)$ is the error covariance of the input estimation process. $K_b(k)$ is the correction gain. $\gamma(k)$ is the weighting factor in the range between 0 and 1. The two functions of $\gamma(k)$ are smoothing and forgetting. The effectiveness of forgetting depends on the value of $\gamma(k)$. $K_b(k)$ gets larger as $\gamma(k)$ gets smaller according to Eq. (36). In the meantime, the effect of forgetting becomes more conspicuous according to Eq. (37). Note that the faster the effect of forgetting is, the lower that of smoothing will be due to the oscillation. The intelligent fuzzy weight-

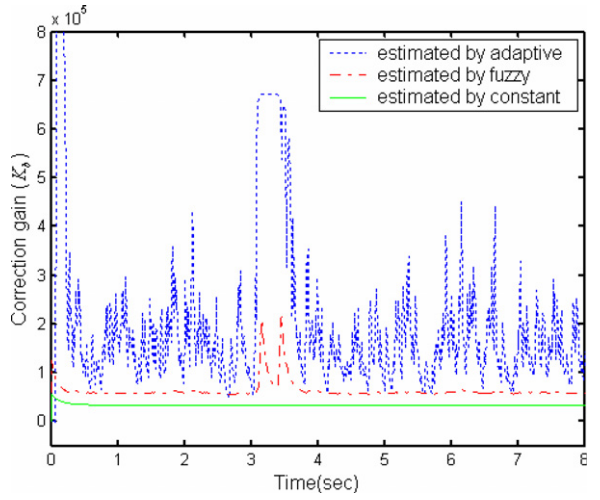

Fig. 5. Comparison of the correction gain using different weighting functions when the input is a single square heat flux wave ($Q = 10^4$, $R = 10^{-8}$).

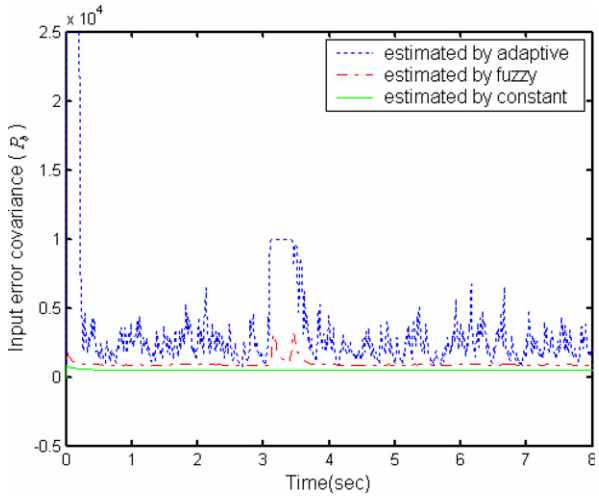

Fig. 6. Comparison of the input error covariance using different weighting functions when the input is a single square heat flux wave ($Q = 10^4$, $R = 10^{-8}$).

ing factor, $\gamma(k)$, is employed to compromise between the upgrade of tracking capability and the loss of estimation precision.

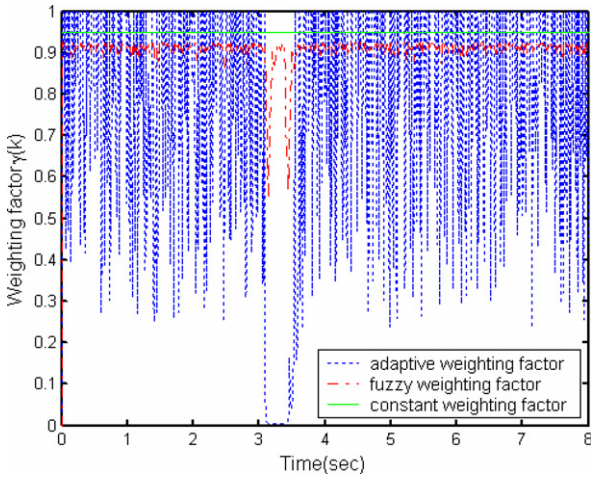

Fig. 7. Comparison of different weighting functions ($Q = 10^4$, $R = 10^{-8}$).

The case has been compared by using the measurement noise covariance matrix, $R = \sigma^2 = 10^{-8}$ and different process noise variance, such as $Q = 1$, 10^2, 10^4 and 10^6 as shown in Fig. 8. It shows that when the process noise variance Q increases, it will influence the estimation resolution. A larger process noise variance will affect the capability of tracking the unknown time-varying heat flux input. As shown in Fig. 8c, the intelligent fuzzy weighted estimator has good performance of estimating the unknown time-varying heat flux in the situation that the variation exits. As shown in Fig. 8d, the adaptive weighted estimator have good tracking performance with the process noise variance, $Q = 10^6$. Nevertheless, it produces overshoot in the estimation process.

Fig. 9 shows the estimation results with the process noise variance fixed ($Q = 10^4$), and different measurement error variances ($R = \sigma^2 = 10^{-4}$, 10^{-6}, 10^{-8} and 10^{-10}) from $t = 0$ s to $t = 8$ s. The result shows that when R is small, the performance of the filter will be better in filtering out the noise. On the contrary, there will be severer fluctuation

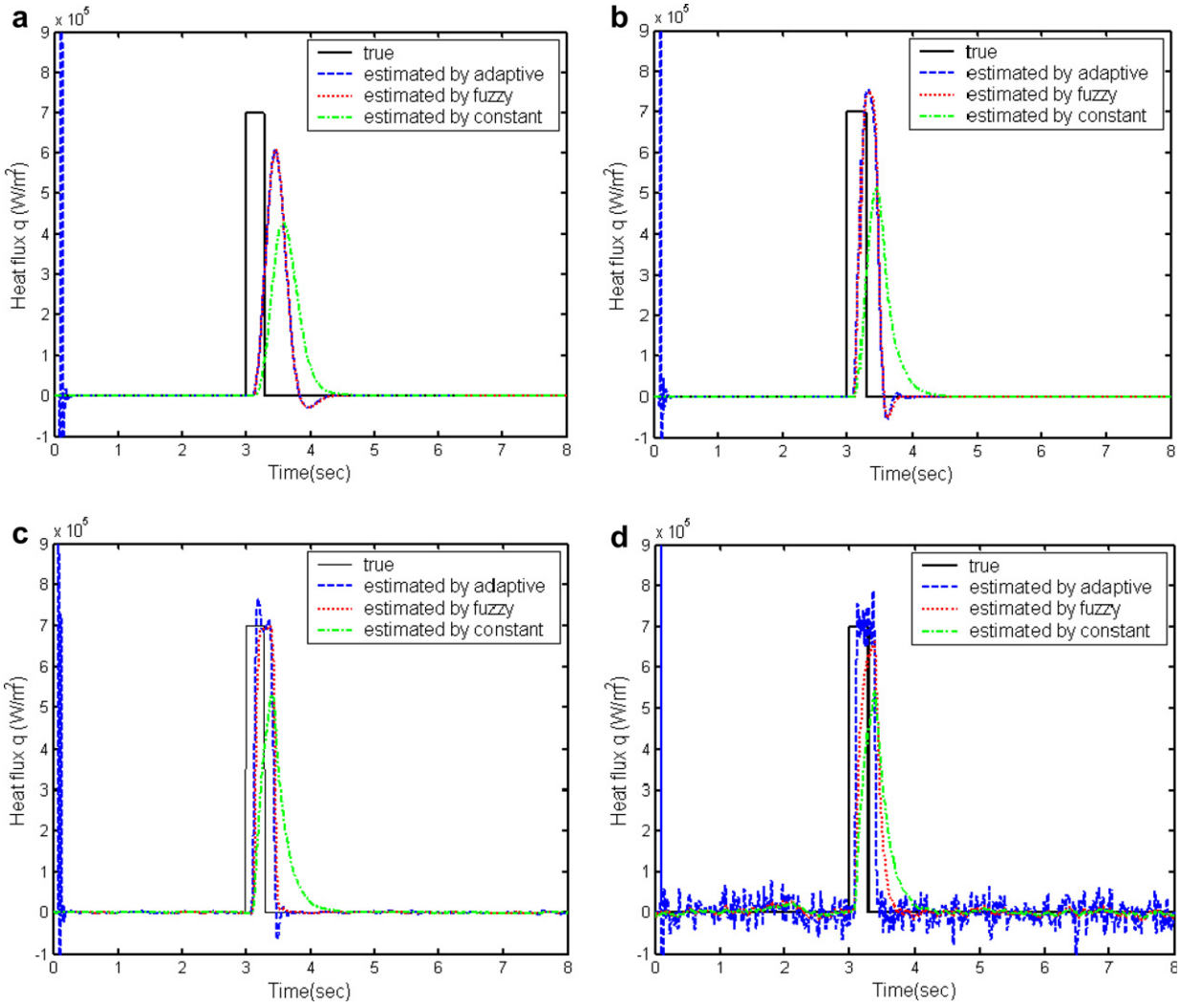

Fig. 8. Effects of various process noise variances ((a) $Q = 1$, (b) $Q = 10^2$, (c) $Q = 10^4$ and (d) $Q = 10^6$) in the input estimation with different weighting functions ($R = 10^{-8}$).

when R increases. In other words, when the measurement variance R increases, the Kalman gain $K(k)$ in Eq. (30) will decrease. The reason is that the corrector uses the new measurement available at kth time step. The correction in Eq. (31) increases, and the Kalman gain $K(k)$ decreases. This makes the estimate closer to the predicted value than the new measurement. According to Fig. 9c, the intelligent fuzzy weighted estimator has great performance in estimating the unknown time-varying heat flux when rapid variation exists. According to Fig. 9d, the adaptive weighted estimator have great tracking performance with the measurement noise variance, $R = 10^{-10}$. The smaller measurement noise variance means that a more precise sensor is in use. However, it is costly to use such an instrument. Besides, it still produces overshoot in the estimation process. On the other hand, the larger measurement error can cause estimation lag and precision degradation. In this research, the temperature measurements on the outer wall are utilized to recursively estimate the temperature on the inner wall. The estimated temperatures on the inner wall can be proven precise by using the backward difference method shown in Fig. 10. The estimated temperature is delayed due to the heat transfer properties. The estimated temperature field distribution is shown in Fig. 11. The influences produced by using different sampling time on estimation results are shown in Fig. 12. The four sets of chosen sampling time,, is 0.1, 0.01, 0.001, and 0.0001 s. The root mean square error of input estimation with different weighting functions and sampling time are shown in Fig. 13. The root mean square error (RMSE) for the estimated heat flux is defined as the following [15]:

$$\mathrm{RMSE} = \left[\frac{1}{D}\sum_{k=1}^{D}(q_k - \hat{q}_k)^2\right]^{\frac{1}{2}}, \tag{48}$$

where D is the total number of time steps. Figs. 12 and 13 show that the better estimation results can be obtained when adopting the smaller sampling time. When the sampling time is 0.01 s, using the constant weighting factor will obtain an estimation result with lower performance. The

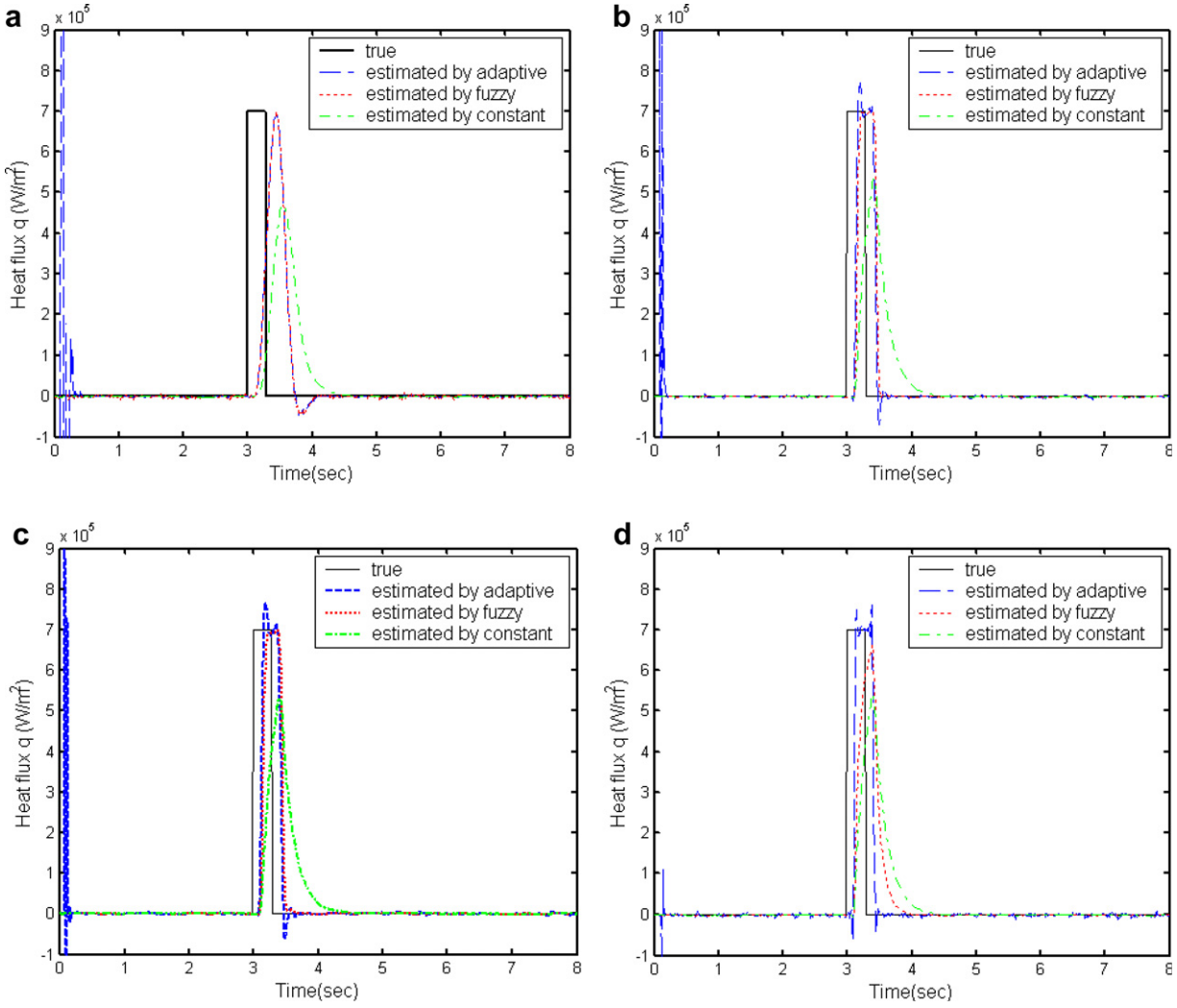

Fig. 9. Effect of various measurement noise covariances ((a) $R = 10^{-4}$, (b) $R = 10^{-6}$, (c) $R = 10^{-8}$ and (d) $R = 10^{-10}$) in the input estimation with different weighting functions ($Q = 10^4$).

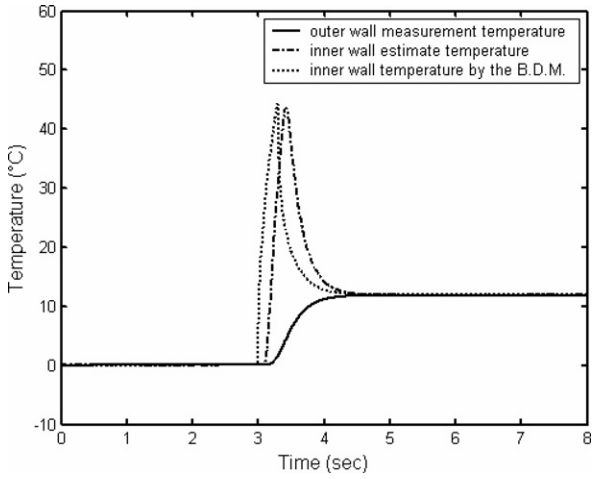

Fig. 10. Comparison of the backward difference method result and estimates on the inner wall and the measurements on the outer wall.

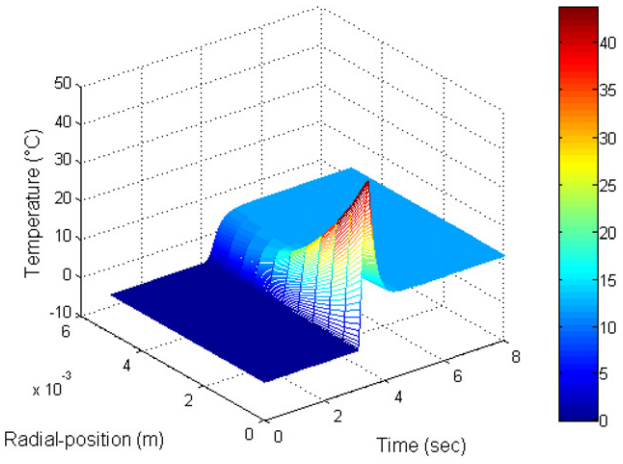

Fig. 11. Temperature estimates in the radial direction.

fuzzy weighted estimator is relatively better. When the sampling time is smaller than 0.01, the estimation result is more precise. However, to take the reaction time of measuring equipments and the computing time of computers into account, the sampling time is set as 0.01 to obtain an acceptable estimation result.

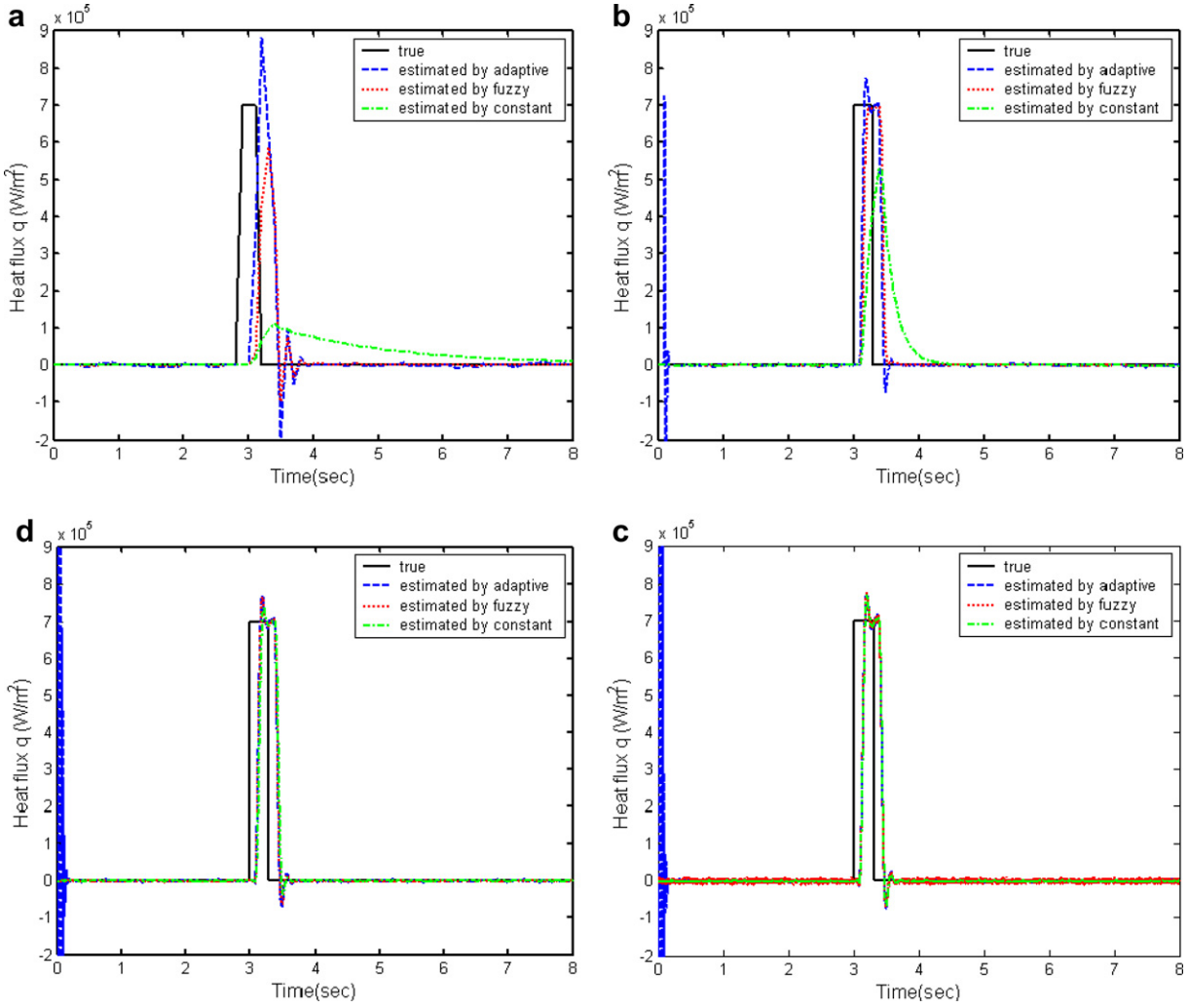

Fig. 12. Effect of various sampling time ((a) $\Delta t = 10^{-1}$, (b) $\Delta t = 10^{-2}$, (c) $\Delta t = 10^{-3}$ and (d) $\Delta t = 10^{-4}$) and weighting functions ($Q = 10^4$, and $R = 10^{-8}$) on the input estimation results.

Example 2. Continuous square waveform for $q(t)$ (W/m^2).

The input heat flux is modeled by a continuous square waveform flowing into the hollow cylinder pipe. The continuous square waveform denotes three rounds in the continuous shots. $q(t)$ is assumed in the form as the following:

$$q(t) = \begin{cases} 7 \times 10^5, & 1 \leqslant t \leqslant 1.5,\ 2 \leqslant t \leqslant 2.5,\ 3 \leqslant t \leqslant 3.5, \\ & 4 \leqslant t \leqslant 4.5,\ 5 \leqslant t \leqslant 5.5,\ 6 \leqslant t \leqslant 6.5, \\ 0, & \text{others.} \end{cases} \tag{49}$$

The thermocouple is located on the outer wall of the hollow cylinder pipe. The process noise covariance matrix, $Q = 10^4$. The measurement noise covariance matrix, $R = \sigma^2 = 10^{-8}$. The estimation results of $q(t)$ using the intelligent fuzzy weighting function, the adaptive weighting function, and the constant weighting factor, $\gamma = 0.95$, are plotted in Fig. 14. The estimation results show that the better convergence is performed by the intelligent fuzzy weighted estimator and the constant weighted estimator rather than the adaptive weighted estimator in the initial stage. The adaptive weighted estimator performs great tracking capability, but it is not capable of reducing the effect due to the measurement noise. On the contrary, the constant weighted estimator has the opposite effect. By using this method, the temperature measurement on the outer wall is adopted to recursively estimate the temperature on the inner wall. The estimated temperatures at the inner wall were validated by the backward difference method shown in Fig. 15. The estimated temperature is delayed because of the heat transfer properties. The estimated temperature field distribution is shown in Fig. 16. The simulation results demonstrate that the proposed method performs great convergence in the initial stage. It is an efficient method in tracking the unknown input and reducing the influence due to the measurement noise.

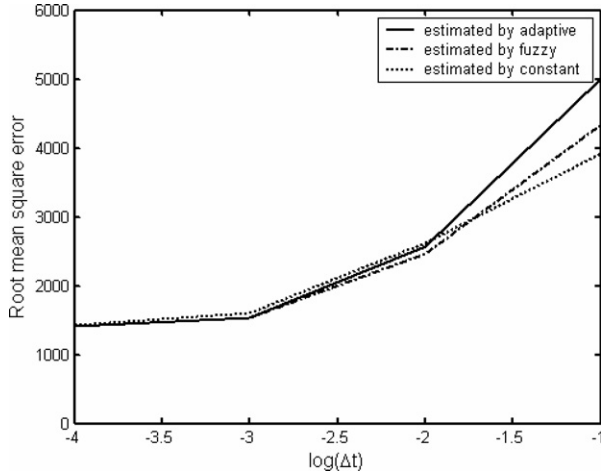

Fig. 13. The root mean square errors of input estimation using different weighting functions and various sampling time ($Q = 10^4$, and $R = 10^{-8}$).

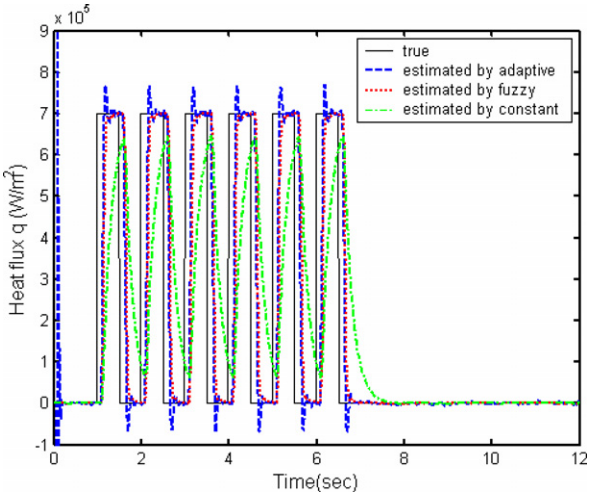

Fig. 14. Comparison of the inverse estimation using different weighting functions when the input is a consecutive square heat flux wave ($Q = 10^4$, $R = 10^{-8}$).

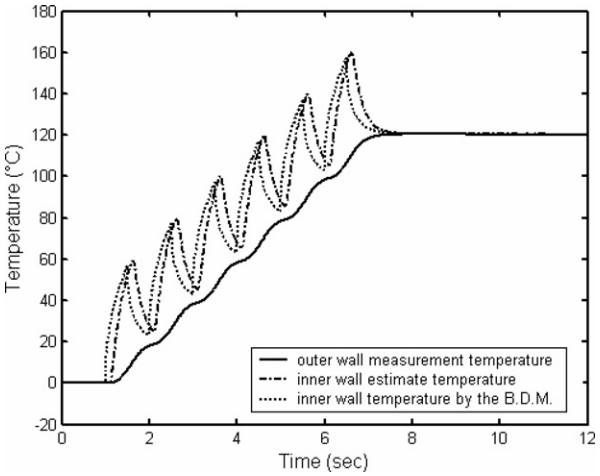

Fig. 15. Comparison of the backward difference method result and estimates on the inner wall and the measurements on the outer wall.

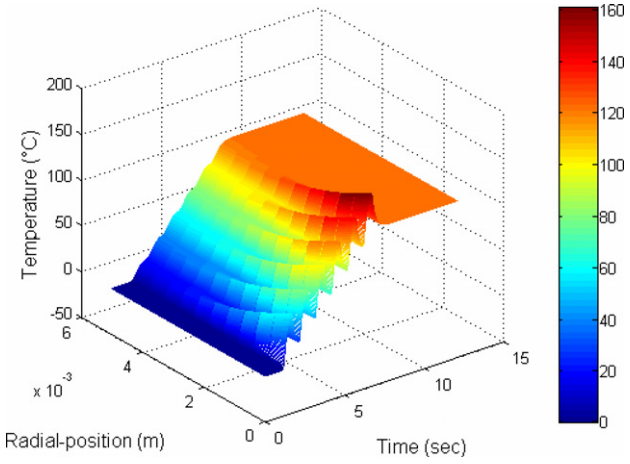

Fig. 16. Temperature estimates in the radial direction.

Example 3. The different levels input heat flux applied on the inner wall in the axial direction [26].

In this example, an inverse method based on the intelligent fuzzy weighted input estimation method including the

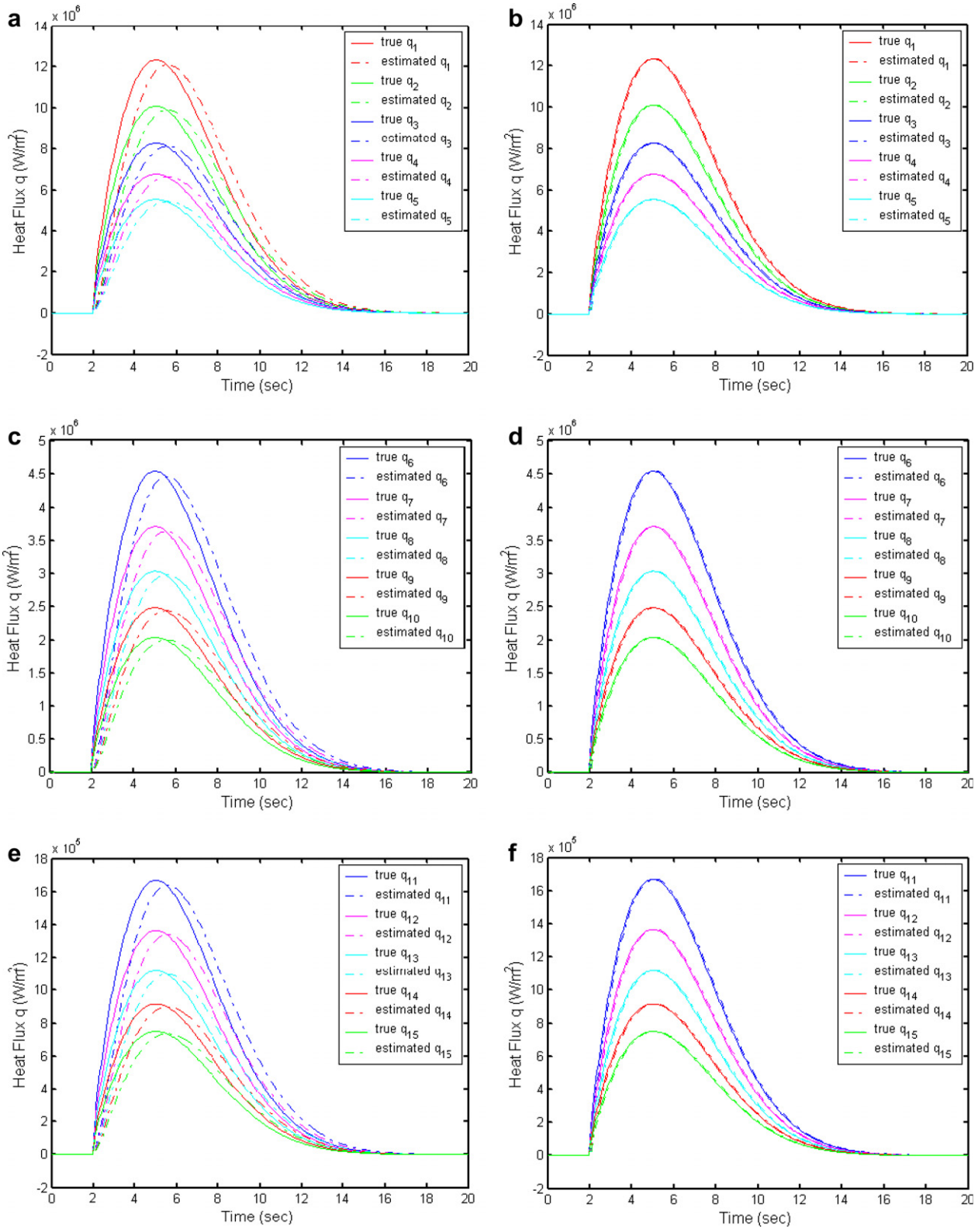

Fig. 17. Comparison of the inverse estimation using the intelligent fuzzy weighting function ((b), (d), and (f)) and the constant weighting factor ((a), (c), and (e)) [26].

finite-element scheme to inverse estimate the unknown heat flux of the 2D gun barrel IHCP is presented. By using the 7.62 mm gun barrel outer wall temperature measurement data, the on-line accuracy is further utilized to inversely estimate the unknown heat flux of the chamber. The simulated uniform and non-uniform heat flux cases are applied to the inner wall of a gun barrel with free convection situation on the outer surface. varies with time and the location on the axis. The relation has already been deliberately derived as follows [26]. In this example, fifteen different input heat flux cases are modeled by using the Weibull distribution form. The unknown input heat flux is assumed as the following:

$$q_i(z,t)=\begin{cases}0, & 0\leqslant t<2,\\ 2\times 10^8\times e^{-z_i}\times\frac{b}{a}\left(\frac{t-2}{a}\right)^{b-1}\times e^{-\left(\frac{t-2}{a}\right)^b}, & 2\leqslant t\leqslant t_f,\\ a=4.8,\quad b=1.8,\quad i=1,2,3,\ldots,14,15,\\ z_i=1+0.2\times(i-1),\quad i=1,2,3,\ldots,14,15.\end{cases}\tag{50}$$

In this case, 15 different input heat flux cases decreases with the exponent form in different positions. The sensors are located at $r=R_o$, *node* $12,24,36,\ldots,156,168,180$. We assume that the measurement noise covariance matrix, $R=\sigma^2=10^{-8}$, process noise variance and the sampling time interval $\Delta t=0.01$ s. The estimation results $q(t)$ of using the intelligent fuzzy weighting function are plotted in Figs. 17b, d, and f, and the constant weighting factor, $\gamma=0.8995$, are plotted in Figs. 17a, c, and e. The simulation results demonstrate that the proposed method performs efficiently in tracking the unknown input. In this case, the 3D heat flux (z,t,q) and inner wall temperature (z,t,q) are plotted in Figs. 18, 19. The simulation results demonstrate that this method applying the measured temperature on 2D gun barrel outer surface can precisely estimate the unknown time-varying heat flux and the temperature field distribution in the chamber in real-time.

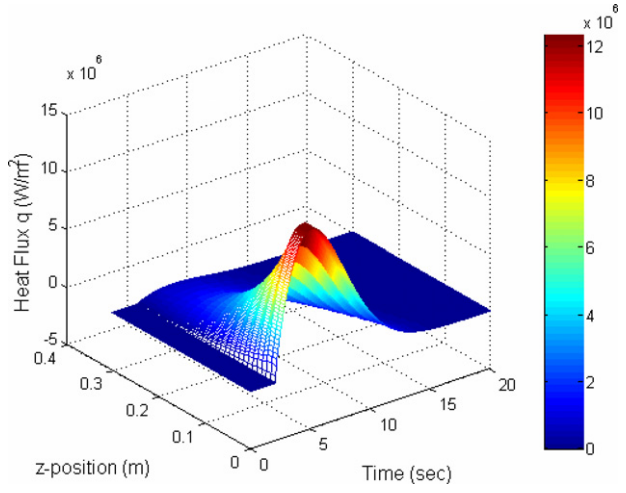

Fig. 18. 3D heat flux (x,y,q) for Example 3.

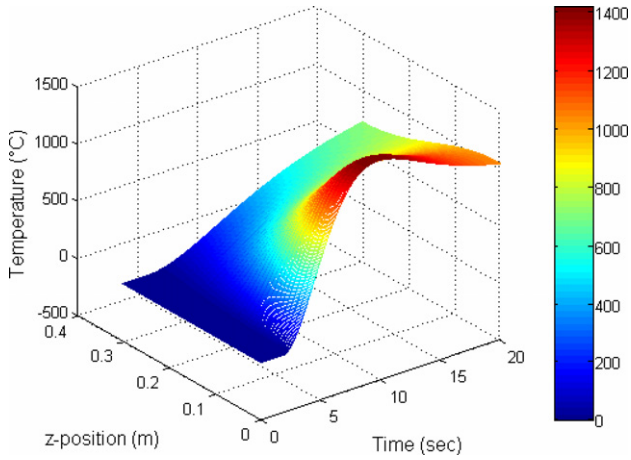

Fig. 19. 3D temperature (z,t,T) on the inner wall for Example 3.

5. Conclusions

A novel intelligent fuzzy weighted on-line input estimation method is developed for the estimation of the unknown time-varying heat flux input with the unpredicted modeling and measurement errors. The proposed intelligent fuzzy weighted estimator is based on the fuzzy logic system to infer the weighting factor. The simulation results show that the proposed method is an efficient adaptive and robust inverse estimation method. Moreover, comparing the constant weighted estimator with the adaptive weighted estimator, the superior estimation capability of the proposed method is verified. Future work will combine the proposed method with Extended Kalman Filter (EKF) for the nonlinear inverse heat conduction problem.

References

[1] J.G. Stolz, Numerical solutions to an inverse problem of heat conduction for simple shapes, ASME J. Heat Transfer 82 (1960) 2–26.
[2] E.P. Scott, J.V. Beck, Analysis of order of the sequential regularization solutions of inverse heat conduction problem, Trans. ASME 111 (1989) 218–224.
[3] K. Miller, Least squares method for ill-posed problems with a prescribed bound, SIAM J. Math. Anal. 1 (1) (1970) 52–74.
[4] O.M. Alifanov, Solution of inverse problem of heat conduction by iteration methods, J. Eng. Phys. 28 (1974) 471–476.
[5] O.M. Alifanov, V.V. Millhailov, Solution of the nonlinear inverse thermal conduction problem, J. Eng. Phys. 35 (6) (1978) 1501–1506.
[6] O.M. Alifanov, E.A. Artyukhin, Regularized numerical solution of nonlinear inverse heat conduction problem, J. Eng. Phys. 29 (1) (1975) 159–164.
[7] V.V. Millhailov, Questions of the convergence of iteration methods of solving the inverse heat conduction problem, J. Eng. Phys. 45 (5) (1983) 1263–1266.
[8] C.H. Huang, M.N. Ozisik, Inverse problem of determining unknown wall heat flux in laminar flow through a parallel plat duct, Numer. Heat Transfer, Part A 21 (1992) 55–70.
[9] C.H. Huang, Y.C. Wang, Inverse problem of controlling the interface velocity in Stefan problems by conjugate gradient method, J. Chin. Inst. Eng. 19 (2) (1996) 247–253.
[10] C.H. Huang, C.W. Chen, A boundary element based inverse-problem in estimating transient boundary conditions with conjugate gradient method, Int. J. Methods Eng. 42 (5) (1998) 943–965.

[11] C.H. Huang, C.C. Tsai, An inverse heat conduction problem of estimating boundary fluxes in an irregular domain with conjugate gradient method, Heat Mass Transfer 34 (1) (1998) 47–54.
[12] H.Y. Li, W.M. Yan, Inverse convection problem for determining wall heat flux in annular duct flow, J. Heat Transfer Trans. ASME 122 (3) (2000) 460–464.
[13] H.Y. Li, W.M. Yan, Identification of wall heat flux for turbulent forced convection by inverse analysis, Int. J. Heat Mass Transfer 46 (6) (2003) 1041–1048.
[14] P.C. Tuan, L.W. Fong, W.T. Huang, Analysis of on-line inverse heat conduction problems, J. Chung Cheng Inst. Technol. 25 (1) (1996) 59–73.
[15] P.C. Tuan, L.W. Fong, W.T. Huang, Application of Kalman filtering with input estimation technique to on-line cylindrical inverse heat conduction problems, JSME Int. J., Ser. B 40 (1) (1997) 126–133.
[16] T.C. Chen, P.C. Tuan, Inverse problem of estimating interface conductance between periodically contacting surfaces using the weighting input estimation method, Numer. Heat Transfer, Part B 41 (5) (2002) 477–492.
[17] T.-C. Chen, C.C. Liu, Inverse estimation of heat flux and temperature in multi-layer gun barrel, Int. J. Heat Mass Transfer 50 (2007) 2060–2068.
[18] P.C. Tuan, S.H. Lee, W.T. Hou, An efficient on-line thermal input estimation method using Kalman filter and recursive least square algorithm, Inverse Prob. Eng. 5 (1997) 309–333.
[19] T. Kailath, An innovations approach to least-squares – part 1: linear filtering in additive white noise, IEEE Trans. Auto. Control AC-13 (1968) 646–655.
[20] P.C. Tuan, W.T. Hou, Adaptive robust weighting input estimation method for the 1-D inverse heat conduction problem, Numer. Heat Transfer, Part B 34 (4) (1998) 439–456.
[21] N. Gerber, M.L. Bundy, Gun barrel heating with heat input during projectile passage, J. Ballist. 12 (4) (1995) 267–281.
[22] J.N. Reddy, Applied Functional Analysis and Variational in Engineering, Malabar, Florida, 1991.
[23] A.H. Jazwinski, Stochastic Processes and Filtering Theory, Academic Press, New York, 1970.
[24] L.X. Wang, Adaptive Fuzzy Systems and Control: Design and Stability Analysis, Prentice-Hall, Englewood Cliffs, NJ, 1994.
[25] Y.A. Cengel, Heat Transfer: A Practical Approach, Second Edition in SI Units, McGraw-Hill, Singapore, 2004.
[26] T.C. Chen, C.C. Liu, Inverse estimation of time varied heat flux and temperature on 2D gun barrel using input estimation method with finite-element scheme, Defence Sci. J. 58 (1) (2008) 57–67.
[27] T.C. Chen, M.H. Lee, Intelligent fuzzy weighted input estimation method for solving inverse gun barrel thermal stress problem, J. Expl. Prop. R.O.C. 23 (2) (2007) 49–68.